Geol Rundsch (1997) 86, Suppl.: S258–S271

ORIGINAL PAPER

A. von Quadt

U–Pb zircon and Sr–Nd–Pb whole-rock investigations from the continental deep drilling (KTB)

Received: 27 August 1996 / Accepted: 4 December 1996

Abstract Among the large number of gabbroic intrusions within the profile of the continental deep drilling (KTB), several types can be distinguished. In this study petrographic, geochemical investigations, conventional U–Pb zircon data and results of Sr–Nd–Pb isotope characteristics of meta-gabbros, amphibolites and felsic rocks are reported. The main results are: U–Pb zircon age data reveal a magmatic Cambro-Ordovician evolution of the Erbendorf-Vohenstrauss zone (ZEV). The range of the ages of magmatic intrusions varies from 496 to 476 Ma, probably as a result of overlap of magmatic and metamorphic processes. Cambro-Ordovician magmatic ages were observed within different mafic (b unit) as well as in variegated units (v unit) of the KTB profile. The Silurian-Devonian metamorphism is dated at around 398 Ma. The Silurian as well as the Variscan metamorphic events apparently did not influence the U–Pb system. The Cambro-Ordovician mafic rocks from the KTB scatter on a ε-Nd evolution diagram. Several meta-gabbros cluster around the $\varepsilon Nd_{T\text{-}500}$ value of +5, but others vary from +8.6 to +0.65 and suggest variable degrees of contamination with continental crust material. A contamination of only 5–10% is required to reduce ε-Nd from +8.6 to approximately +5. According to the REE patterns and the Sr–Nd–Pb data, the mafic rocks could either derive from an enriched mantle source or else their protolith magma originated from a depleted mantle and was contaminated by continental crust. The data for the mafic rocks of the ZEV are in accord with observation by other authors regarding the evolution of the Late-Proterozoic to Early Palaeozoic magmatism in the Bohemian massif.

A. von Quadt
Institut für Isotopengeologie und Mineralische Rohstoffe,
ETH-Zürich, Sonneggstr. 5, CH-8092 Zürich, Switzerland
Fax: + + 41-1–632 1179
E-mail: quadt@erdw.ethz.ch

Key words U–Pb zircon · Meta-gabbros · KTB · Bohemian massif · Cambro-Ordovician

Introduction

In this paper, U–Pb zircon, Pb–Sr–Nd isotope and major, trace and REE data of pre-Variscan rocks (meta-gabbros, para-/orthogneisses, amphibolites) are presented from the Variscan basement of NE Bavaria; these include only rocks from the continental deep drilling core. The pre-Variscan evolution of the Bohemian massif – integrated into the Variscan basement – is partly established by geochronological studies (see Geological background). In such a polymetamorphic context, the best – if not the only – possibility to obtain reliable magmatic crystallisation ages is by the U–Pb method applied to zircon and/or other accessory U-bearing minerals.

The KTB drill site lies in the northern part of the Erbendorf-Vohenstrauss zone (ZEV). The ZEV is a small NW- to SE-trending metamorphic unit composed of paragneisses and different types of mafic rocks. In the north, the ZEV is bordered by mafic and ultramafic rocks of the Erbendorf greenschist zone and different meta-sediments and meta-volcanics. In the east and south the ZEV borders against the high-grade rocks of the Moldanubian unit. The contacts between

Fig. 1a, b Sketch of the western part of the Bohemian massif. *MN* Moldanubian zone; *ST* Saxothuringian zone; *MM* Münchberg massif; *ZEV* Zone of Erbendorf-Vohenstrauss; *ZTT* Zone of Tepla-Taus; *ZTM* Zone of Tirschenreuth-Mähring; *W* Winklarn, high-pressure rocks; *1, 2* lower nappes; *3* Saxothuringian; *4* Moldanubian; *5* late-/post-Variscan granites; *6* KTB drill site; *7* Franconian Line; **c** Lithological column of the KTB Hauptbohrung (HB) and geological NE–SW cross section (Hirschmann et al. 1994). The numbers on the left side of the profile refer to the sample numbers in Table 1

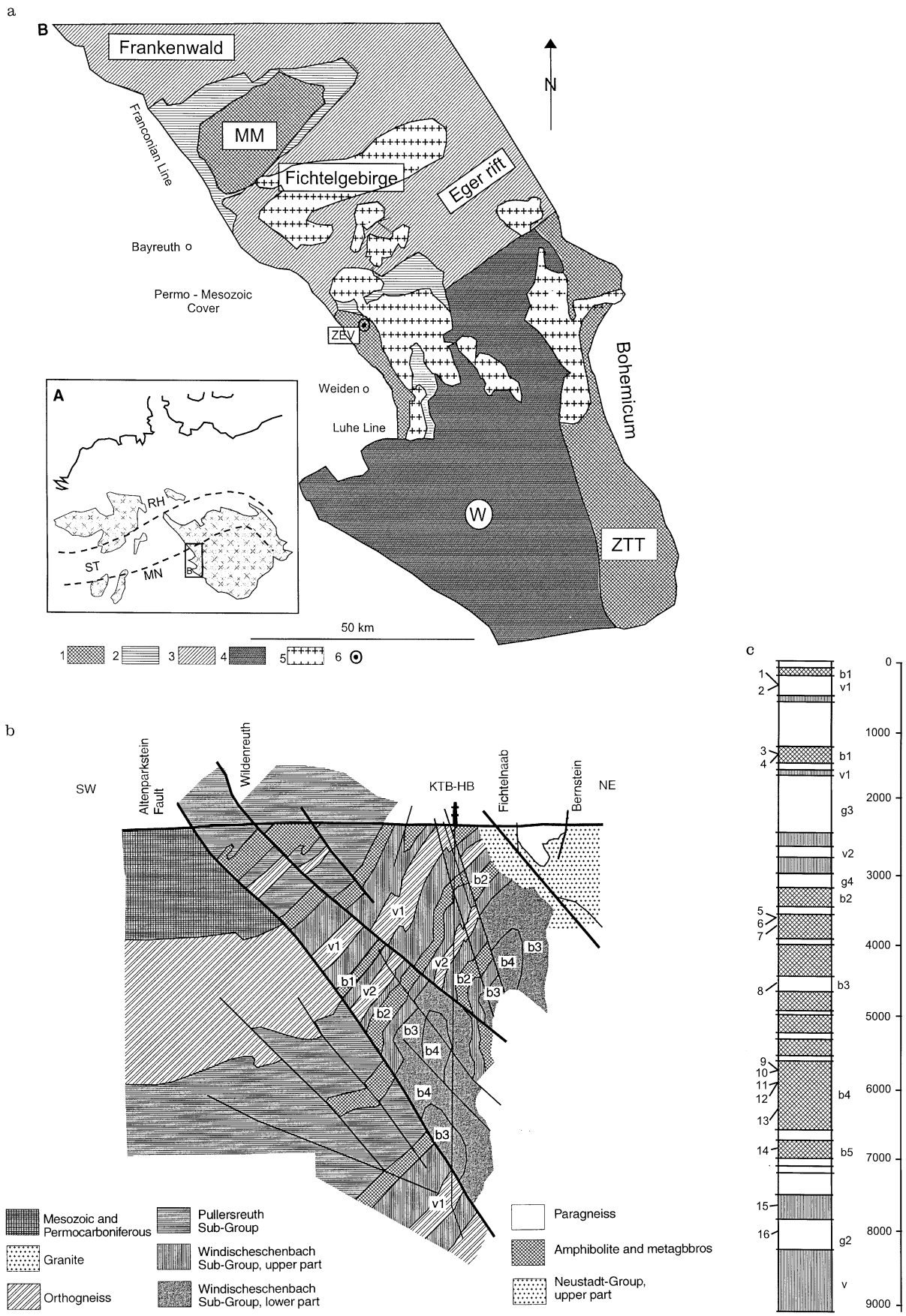
a
B
Frankenwald
MM
Fichtelgebirge
Franconian Line
Eger rift
N
Bayreuth o
Permo - Mesozoic
Cover
ZEV
Weiden o
Luhe Line
Bohemicum
W
ZTT
A
RH
ST
MN
50 km
1
2
3
4
5
6
b
SW
Altenparkstein
Fault
Wildenreuth
KTB-HB
Fichtelnaab
Bernstein
NE
v1
b1
v2
b2
b3
b4
Mesozoic and
Permocarboniferous
Granite
Orthogneiss
Pullersreuth
Sub-Group
Windischeschenbach
Sub-Group, upper part
Windischeschenbach
Sub-Group, lower part
Paragneiss
Amphibolite and metagbbros
Neustadt-Group,
upper part
c
b1
v1
g3
v2
g4
b2
b3
b4
b5
g2
v
0
1000
2000
3000
4000
5000
6000
7000
8000
9000

them are marked by late Variscan dioritic and granitic intrusions (Steinwald, Falkenberg, Leuchtenberg). In the SW, the basement units are thrust upon the Permo-Carboniferous and Mesozoic sediments by the fault system of the Franconian lineament (Fig. 1). The northern part of the ZEV can be subdivided into an upper gneiss-rich unit (Püllersreuth subgroup; Hirschmann 1993) and a lower unit with abundant mafic rocks (Windischeschenbach subgroup). Both units dip to the southwest. The KTB drill site is situated in the lower unit and comprises the Vorbohrung (VB) and the Hauptbohrung (HB). Due to technical problems during the drilling operation several separate holes exist (Hirschmann et al., in press).

The principle aim of this study was to define the protolith age for mafic rocks, and furthermore, by combining multi-isotope data of mafic rocks, to examine the relative importance of mantle, crustal and mixed magma sources as a function of time. The protolith age information as well as the source data are compared with other mafic complexes in Central Europe, and the geodynamic implications for the evolution of the Variscan basement are discussed.

Geological background

The Moldanubian basement of the Bohemian massif (BM) contains numerous undated meta-gabbros and other mafic/ultramafic rocks (Fig. 1). They are associated with metamorphic rocks of igneous and/or sedimentary origin. For most of these occurrences it is typical that the associated country rocks do not reflect the same metamorphic history as the igneous mafic rocks. The country rocks of the Moldanubian were metamorphosed at pressures between 3 and 4.5 kbar and temperatures between 670 and 700 °C (Blümel 1983, 1984). Based on conventional as well as on ion-probe data on detrital zircons, the ages of the meta-sedimentary rocks range up to 3.8 Ga (Gebauer et al. 1989). The deposition of the meta-sedimentary rocks took place after the Pan-African (or Cadomian) orogenic cycle, 550 Ma ago. The first metamorphic overprint of these sediments took place during the Ordovician. Different metamorphic ages have been obtained which probably reflect the presence of different tectonic units. Grauert et al. (1974) obtained 488 $\pm$ 20 Ma for the Ordovician metamorphism of rocks from the low-pressure unit and Gebauer et al. (1989) reported a similar age of 459 $\pm$8 Ma for the anatexis of paragneisses from the Regensburg Forest. Teufel (1988) dated monazites from cordierite-bearing gneisses and the age of 455 $\pm$4 Ma may reflect an early high-grade metamorphic event. In the SW part of the BM the intrusion of the layered mafic/ultramafic Neukirchen-Kdyne complex has been dated at 511 $\pm$3 Ma (Gebauer 1993). An age of 494 $\pm$2 Ma on another mafic complex in the NE part of the BM, the Rudawy Janowickie terrane, reflects magmatic intrusion (Oliver et al. 1993). Bowes and Aftialon (1991) reported an Ordovician intrusion age (496 $\pm$1 Ma) of meta-gabbros from the Marianske Lasne complex, a geological unit close to the NE of the KTB.

The target area occupies the western margin of the BM (Fig. 1). The zone of ZEV contains amphibolites, paragneisses, orthogneisses, and meta-pegmatites, over printed by variable degrees of metamorphism. Two granites in the east of the ZEV, the Leuchtenberg and Falkenberg granite, intruded at 326 $\pm$4 and 311 $\pm$ 8 Ma (Siebel et al. 1995).

As high-pressure events are preserved and recognised in mafic assemblages, dating of such rocks might yield protolith ages as well as the age of the high-pressure event. Geochemical data and Nd–Sr–Pb isotopic data are expected to give information on the geotectonic environment of their protoliths. An oceanic source would imply tectonic transport and stacking within the meta-sedimentary rocks.

The metamorphic rocks of the VB and HB comprise amphibolites, meta-gabbros, hornblende gneisses and paragneisses which may occur interlayered by several alternations. The upper section of the profile ($<$3160 m) is characterised by paragneisses, amphibolites and mafic-felsic units. The middle section (3160–7260 m) is represented by amphibolites with minor intercalations of meta-gabbros and hornblende gneisses. The lower section (7260–9100 m) again consists of alternations of amphibolites and paragneisses. The boundaries between all major units are marked by cataclastic faults. As outlined in Fig. 1c the profile of the KTB drill core can be subdivided into lithological characteristic units: gneiss unit (g), variegated units (v) and metabasic units (b).

The individual gneiss units differ by the amount and distribution of metapelitic and metapsammitic paragneisses and minor intercalations of mafic rocks. The variegated unit occurs in the upper and lower part of the profile (Fig. 1b) and contains alkaline marble-bearing amphibolites, metatrachytic metabasites, alkaline amphibolites and gneisses. The metabasic unit is the dominant part of the middle section and contains garnet amphibolites, meta-gabbros and minor intercalations of gneisses. All metamorphic units (g, v, b) are crosscut by mafic and felsic dykes related to the late-Variscan granitoids (Siebel et al. 1995).

Analytical methods

U–Pb zircon dissolution and chemical separation were performed according to the method described by Manshes et al. (1984) and von Quadt (1992); total Pb blanks amounted to 30 and 70 pg. Pb was loaded on a single Re filament with H_3PO_4 and silica gel; U was loaded on a double Re filament with HNO_3, and if

single zircons were analysed, on the same filament as Pb. U and Pb concentration were determined using a mixed $^{205}Pb/^{235}U$ spike. Linear fractionation effects equivalent to 0.13 ±0.005% per mass unit were corrected, based on repeated measurements of the NBS SRM 981 lead standard. $^{206}Pb/^{204}Pb$ ratios greater than 3000 were measured by using an electron multiplier. The reproducibility of measurements of the standard was 0.1% for $^{206}Pb/^{204}Pb$ and $^{207}Pb/^{204}Pb$ and 0.2% for the $^{208}Pb/^{204}Pb$ ratio (2 sigma). The reproducibility of an internal laboratory zircon standard was 0.8% for $^{206}Pb/^{238}U$, 1.4% for $^{207}Pb/^{235}U$ and 0.5% for $^{207}Pb/^{206}Pb$ ratio. The error ellipses on the concordia diagram were calculated for individual fractions using 2-sigma errors (Roddick 1987) and regression lines were calculated using the method of Ludwig (1980).

The procedures for Sm, Nd and REE whole-rock and mineral analyses are modified from those reported by Richard et al. (1976). After dissolution in open beakers (HF cold, 24 h), the samples were treated in Teflon (DuPont) bombs using $HF–HNO_3–HClO_4$. The samples were spiked with either a highly enriched REE tracer or a mixed $^{150}Nd–^{149}Sm$ tracer. A cation-exchange column was used to concentrate the REE; Sm–Nd and REE were separated on a second column containing Teflon powder coated with di-2-ethyl-hexyl-orthophosphoric acid. No Sm interferences were observed in the Nd measurement. The REE elements were loaded with HCl on different filament assemblies (single, double, triple). All isotope measurements were performed (dynamic mode) on a Finnigan MAT 261 mass spectrometer using a fixed multicollector system. Several REE analyses (see Table 2) were performed on an ICP-MS (Perkin Elmer) at the EMPA (Eidgenössische Material- und Prüfungs Anstalt).

The Nd-isotopic ratios were normalised to $^{146}Nd/^{144}Nd = 0.7219$. The reproducibility of the data was estimated by measuring the La Jolla Standard. The mean of 17 runs during this work was $^{143}Nd/^{144}Nd = 0.512846 \pm 7$ (95% CI). Analysis of BHVO-I yielded a $^{143}Nd/^{144}Nd$ ratio of 0.512991 ± 14 (14 measurements). The reproducibility of the $^{147}Sm/^{144}Nd$ ratio was estimated from replicate analyses to be within 0.17%. The model ages, T_{DM} and T_{CH}, were calculated to be 0.1967, with $^{147}Sm/^{144}Nd = 0.213$, and 0.512638, with $^{143}Nd/^{144}Nd = 0.513150$, assuming a depleted mantle evolving linearly with time (Goldstein et al. 1984).

Sample description

U–Pb zircon analyses have been performed on several meta-gabbros, one amphibolite and two gneisses from the lower levels of the KTB profile (Fig. 1b). Nd–Sr–Pb whole-rock and mineral analyses were made on gneisses, amphibolites and meta-gabbros.

The meta-gabbros are coarse-grained rocks with partly preserved ophitic structures. These mafic rocks consist mainly of clinopyroxene, garnet, amphibolite and plagioclase. Minor amounts of biotite, rutile, zircon and pyrite are observed (Table 1). The main forming minerals in the amphibolites are hornblende, plagioclase, garnet and minor quartz and biotite. The accessories are apatite, zircon, sphene and rutile. The garnet contents are variable and the grain size varies from 0.1 to 0.5 mm. The paragneisses consist of plagioclase, quartz, biotite, garnet, sillimanite and muscovite. Depending on their whole-rock alteration

Table 1 Sample description. qtz quartz; bio biotite; chl chlorite; zr zircon; grt garnet; hbl hornblende; sph sphene; epi epidote; kf kalifeldspar; ap apatite; sil sillimanite; seri sericite; mus muscovite

Sample no.	Sample	Sample description	Depths m	Rock type
(see Fig. 1c)				
1	39A5a	qtz, kf, plag, bio, chl, zr, grt	256.67	Chlorite gneiss
2	47A45	qtz, plag, bio, hbl, grt	324.37	Chlorite gneiss
3	264, C1F, C1g, H10p(263)	cpx, grt, amph, plag, ±bio, qtz, ap, zr	1262–1265	Meta-gabbro
4	280, C2h, F2y, E2x	cpx, grt, amph, plag, ±bio, qtz, ap, zr	1334–1336	Meta-gabbro
5	882, H4ba	cpx, grt, amph, plag, ±bio, qtz, ap, zr	3606	Meta-gabbro
6	911, 1ab, 1ac, E1ad, E1gfk	cpx, grt, amph, plag, ±bio, qtz, ap, zr	3718	Meta-gabbro
7	939, F1HK, E1GK	cpx, grt, amph, plag, ±bio, qtz, ap, zr	3834	Meta-gabbro
8	H009, F39	cpx, grt, amph, plag, ±bio, qtz, ap, zr	4688	Meta-gabbro
9	H025, A2a, 2b, 3T, 4T, B5d	cpx, grt, amph, plag, ±bio, qtz, ap, zr	6244–6245	Meta-gabbro
10	H025, D13a, D12	cpx, grt, amph, plag, ±bio, qtz, ap, zr	6247	Meta-gabbro
11	H026, A1a, 1c, 4c, B6a	cpx, grt, amph, plag, ±bio, qtz, ap, zr	6304–6305	Meta-gabbro
12	H027A1a, 2S	cpx, grt, amph, plag, ±bio, qtz, ap, zr	6355–6356	Meta-gabbro
13	H030D1	hbl, plag, grt, ±qtz, bio, kf, sph, ap	6668	Amphibolite/meta-gabbro
14	H031A1K	plag, qtz, bio, grt, sil, mus, ±chl, seri	7011	Hornblende-gneiss
15	H033A1T	hbl, plag, grt, ±qtz, bio, kf, sph, ap	7400.30	Amphibolite
16	H034A3j	plag, qtz, bio, grt, sil, mus, ±chl, seri	8071.88	Garnet–sil biotite gneiss

chlorite, sericite and others are observed. Intensely altered rocks were collected from different depths at 256 and 324 m (Table 1). These altered rocks are called chlorite gneiss or chlorite fels.

Results

Geochemical data

Major, trace and REE data for the studied rocks are listed in Table 2. The samples comprise amphibolites retrograded to different degrees, gneisses and meta-gabbros. Selected trace element data are plotted in Fig. 2. Most of the meta-gabbros represent a basaltic liquid composition. When plotted on different discrimination diagrams, e.g. Cr–Ti, Ti–Zr, Nb/Y–Zr/TiO_2, the meta-gabbros fall into either the ocean floor basalt (OFB) or island arc basalt fields (IAT; Pearce 1982; Pearce and Norry 1979).

Normalised REE data for selected samples are plotted in Fig. 3. Most of the REE patterns are enriched in LREE with one exception, sample H025b, which is slightly depleted in LREE; meta-gabbros from the Vorbohrung (VB; Fig. 3a) have an $(La/Lu)_n$ ratio of 3.6, whereas the meta-gabbros from the Hauptbohrung (HB) show a $(La/Lu)_n$ ratio of 2.4 (Fig. 3b). The amphibolite (Fig. 3c, H033) and the gneisses (Fig. 3c, VB39A, VB47B) have a slightly enriched LREE part. Two chlorite gneisses (Fig. 3c, VB39A, VB 47B) have the highest REE concentration, $(La/Lu)_n$ ratios of 8.4 and 19.9 and negative Eu anomalies. The high $(La/Lu)_n$ ratio of the meta-gabbros from the VB is not combined with a fractionation process (Table 2). All distribution patterns of the mafic rocks point to a homogeneous source such as an enriched mantle, probably contamination with Cadomian crust material.

The extended spider diagrams show a very homogeneous pattern for the meta-gabbros of the VB (Fig. 2a). The meta-gabbros from the HB (Fig. 2b) display similar patterns, but several elements (La, Ce, Sr, Zr) are scattered. Lead, potassium and strontium are strongly enriched relative to an N-type MORB reference. The two gneisses (VB39A, VB47B) are extremely enriched in Zr, Pb, K and Nb (Fig. 2c), whereas the patterns of the other gneisses and amphibolites are more heterogeneous probably reflecting a mixture from different source material.

Sr–Nd–Pb data

Sr, Nd and Pb isotopic data (Tables 3, 4) are summarised in Fig. 4, which presents the $^{143}Nd/^{144}Nd$ against $^{206}Pb/^{204}Pb$ and $^{207}Pb/^{204}Pb$ against $^{206}Pb/^{204}Pb$ ratios. The Nd–Pb plot (modified after Zindler and Hart 1986) indicates possible source fields for different rock systems (Fig. 4a). Meta-gabbros span an ε-Nd range between 0.65 and 8.6. The highest value occurs in sample H026 (Table 4), a flat REE pattern and a more primitive rock type than the others. The two amphibolitic rocks (H033: -10.55; H030: -6.82) as well as the hornblende gneiss (H031: -0.69) have very low ε-Nd values and were probably contaminated with a meta-sedimentary source rock. The felsic rock type shows a wide range within the ε-Nd values from 0.21 to -16.9 (Table 4). The mean ε-Nd value for the mafic rocks cluster around 5.1. Similar values are obtained for mafic/ultramafic rocks from the Moldanubian part of the BM, e.g. Winklarn (von Quadt and Gebauer 1993), Neukirchen (Miethig 1995), Saxonian Granulite Massif (von Quadt 1994) and Münchberg Gneiss massif (Stosch et al. 1989). Most of these mafic rocks reveal a considerable increase in Sm/Nd with differentiation, but no isochron can be calculated for all the samples. The strontium system may be disturbed in most rock samples, but those rocks with negative ε-Nd values show the expected high $^{87}Sr/^{86}Sr$ ratios (Table 4). Based on their Nd–Pb pattern the source for the mafic rocks display a mixture between a depleted mantle source (DMMA) and an enriched source type (EM-II).

In Fig. 4b the mafic rocks are plotted in a $^{206}Pb/^{204}Pb$ vs $^{207}Pb/^{204}Pb$ diagram; all data points were corrected for T-500 and T-300 Ma. All meta-gabbros are characterised by a similar source type, expressed by a very constant μ-value of 9.554 ± 0.032. Higher μ-values (Table 3) correlate with lower ε-Nd values. A best-fit line through the field of mafic rocks on the $^{206}Pb/^{204}Pb$–$^{207}Pb/^{204}Pb$ system point to a homogenisation during the magmatic evolution of these rocks in Cambro-Ordovician time. A factor analysis for different corrected Pb data demonstrate that the time of 500 Ma has the best homogenisation for the whole rocks. The U–Th–Pb whole-rock analyses of the meta-gabbros show variable Th/U ratios from 1.64 to 5.61, the amphibolites from 0.4 to 2.1 and the chlorite gneisses from 0.67 to 2.3. The lower Th/U ratios of the more felsic rocks is related to an increase in U concentrations.

Whole-rock/garnet data

Two mafic rocks were selected for Sm/Nd geochronology using whole rock and garnet (Table 4, samples 280, 939). No other mineral is suitable to detect the post-magmatic overprint. The garnets were separated based on their colour, but this selection did not increase the spread of $^{147}Sm/^{144}Nd$. The whole-rock garnet pairs reflect the time of the metamorphic overprint with ages of 398 ± 12 and 392 ± 20 Ma (Table 4). Similar metamorphic ages have been reported for other KTB rock units based on Ar–Ar and K–Ar measurements on

Table 2 Major elements (wt.%), trace and REE elements (ppm)

Sample	264	280	882	911	939	H009	H025a	H025b	H026	H027	H030	H031	H033	H034	39A5A	[1]47A45
SiO_2	47.64	46.82	48.02	47.34	47.99	48.66	46.84	46.13	47.00	49.13	54.66	59.37	45.02	56.34	60.73	60.69
TiO_2	1.37	1.30	1.45	1.27	1.58	2.27	0.98	0.96	1.25	2.53	0.89	1.36	2.75	1.69	0.23	0.26
Al_2O_3	17.66	15.41	17.23	14.50	15.66	14.87	19.91	17.2	18.38	16.57	19.03	16.69	14.18	15.78	17.29	17.91
Fe_2O_3	9.02	10.33	10.32	10.81	10.66	12.97	9.46	10.22	10.1	12.07	8.70	8.65	11.78	10.01	6.92	6.77
MnO	0.15	0.17	0.16	0.17	0.17	0.22	0.13	0.13	0.16	0.27	0.14	0.15	0.18	0.16	0.13	0.21
MgO	8.07	10.67	7.82	11.24	7.20	6.54	8.75	10.85	9.27	6.61	4.29	3.95	6.87	4.16	0.42	1.01
CaO	10.06	9.24	9.63	8.47	9.44	9.03	10.14	10.07	10.21	7.91	5.32	4.40	13.2	6.26	2.39	3.91
Na_2O	2.71	2.37	2.85	2.09	2.68	2.59	2.35	1.99	2.00	2.76	4.16	2.90	3.14	1.84	3.45	5.41
K_2O	0.59	0.47	0.49	0.56	0.65	0.73	0.41	0.70	0.25	0.46	1.57	1.74	0.75	2.47	6.53	3.13
P_2O_5	0.18	0.14	0.21	0.18	0.23	0.36	0.06	0.04	0.11	0.15	0.23	0.20	0.72	0.37	0.10	0.12
H_2O	2.03	2.31	1.01	2.25	0.65	0.74	0.42	1.05	0.80	0.75	0.85	0.38	1.10	0.25	0.66	1.15
Total	99.54	99.32	99.21	98.98	96.94	99.00	99.39	99.39	99.59	99.26	99.84	99.79	99.72	99.33	99.46	100.6
F	342	346	315	309	292											
Ba	141	111	110	142	104	334	83	151	62	133	496	648	308	516	474	404
Rb	13	18	13	18	17	15	11	20	7	4.41	7.66	42	8	52	21	49
Sr	296	199	279	151	182	194	361	231	310	65.4	73.4	267	303	189	184	213
Y	25	25	27	29	35	36	9	10	17	3.65	1.71	17	12	24	109	122
Zr	97	97	111	94	128	210	27	78	88	62	143	176	208	158	1269	1516
V	236	205	168	178	208	293	138	168	136	382	143	217	192	232	22	20
Cr	344	445	101	492	242	197	297	347	266	179	6	118	220	100	6	6
Ni	110	246	71	216	70	56	125	195	208	31	36	44	118	49	3	3
Co	40	46	49	56	45	61	60	56	55	50	12	32	60	17	26	14
Cu	46	30	30	22	24	5	59	8	29	12	23	7	6	16	3	3
Zn	63	73	77	81	82	121	63	101	71	99	64	120	94	117	214	184
Sc	34	33	27	30	37	47	18	21	27	41	21	27	26	31	2	2
S	905	308	912	680	655	554	1354	327	469	1791	251	1291	160	9101	96	50
Be	0.61	0.64	0.64	0.64	0.85	1.55	0.51	4.11	0.54	0.78	1.44	1.12	1.11	2.32	4.71	2.09
Ga	14	14	17	14	17	19	15	17	14	16	15	20	17	20	40	42
Ge	1.44	1.27	1.47	1.27	1.64	1.78	1.39	1.95	1.41	1.81	0.829	1.19	0.939	1.882	1.01	1.33
Nb	4.4	6.6	4.5	3.3	3.9	4	4	4	4	4	4.79	12.1	35.3	21.9	103	103
Hf	1.18	1.46	1.16	1.25	0.97	1.17	0.54	0.91	0.62	0.67	0.298	0.356	0.75	0.362	2.59	0.28
Ta	2.0	2.56	2.4	2.13	0.80	1.36	0.62	0.94	0.89	2.19	0.357	0.826	2.08	1.563	2.83	4.27
La	4.07	3.94	8.49	4.59	7.18	9.43	2.76	0.95	4.60	5.42	1.762	2.95	6.72	8.92	3.13	13.7
Ce	9.42	9.58	19.42	8.61	16.1	28.3	7.65	3.08	12.37	15.93	6.90	22.6	30.4	35.1	115	158
Pr						3.72	0.99	0.64	1.74	2.21	0.57	0.79	1.66	2.45	8.41	3.89
Nd	7.16	7.62	12.88	8.55	11.7	18.58	5.03	2.75	8.56	8.91	2.446	3.06	6.72	10.0	31.8	13.9
Sm	1.73	1.82	3.34	2.31	3.22	5.32	1.29	1.06	2.35	2.47	0.55	0.62	1.37	2.22	6.56	2.29
Eu	0.567	0.620	1.16	0.749	0.990	1.63	0.79	0.69	1.11	1.63	0.184	0.18	0.48	0.77	0.59	0.17
Gd	1.93	1.97	3.81	2.69	3.95	7.39	1.72	1.86	3.47	3.46	0.494	0.59	1.34	2.37	6.16	1.78
Tb						1.03	0.24	0.23	0.48	0.48	0.07	0.09	0.20	0.38	1.02	0.32
Er	0.919	0.919	1.92	1.44	2.07	3.74	0.82	0.85	1.68	1.88	0.202	0.25	0.50	1.21	3.09	0.74
Ho						1.35	0.31	0.34	0.61	0.65	0.07	0.09	0.19	0.65	1.12	0.28
Dy	1.59	1.61	3.39	2.56	3.59	6.52	1.46	1.71	2.99	3.12	0.372	0.47	1.01	2.16	5.69	1.49
Tm						0.53	0.12	0.14	0.24	0.28	0.03	0.04	0.07	0.17	0.43	0.09
Yb	0.639	0.719	1.49	1.13	1.78	2.91	0.65	0.89	1.42	1.83	0.186	0.22	0.42	1.16	2.78	0.55
Lu	0.110	0.089	0.240	0.160	0.259	0.44	0.11	0.12	0.20	0.26	0.027	0.032	0.056	0.17	0.38	0.071

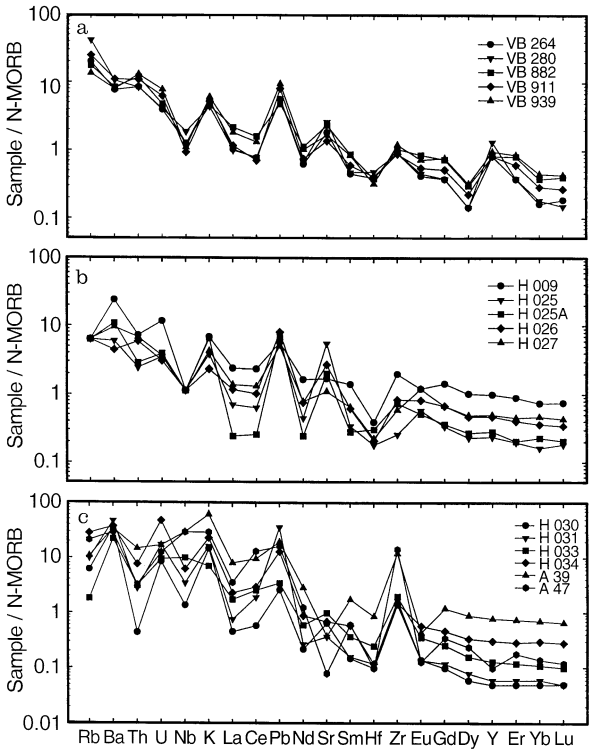

Fig. 2a–c Normalised trace element data for the meta-gabbros, gneisses and amphibolites

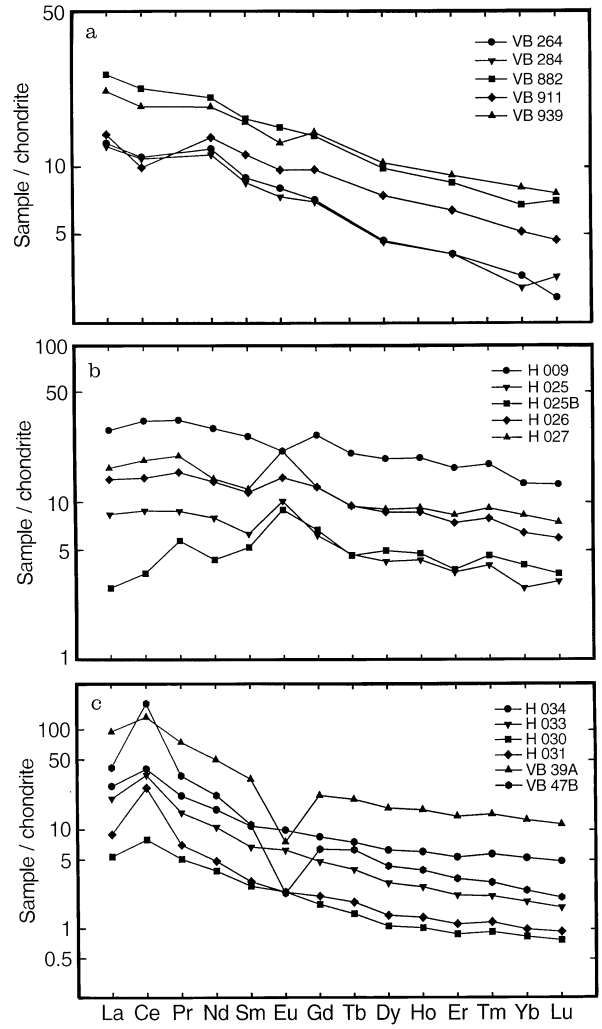

Fig. 3a–c The REE plot for the meta-gabbros, gneisses and amphibolites

muscovites (Wemmer and Ahrendt 1994; Henjes-Kunst et al. 1994; Ahrendt et al. this volume) and for rocks of the ZEV (Kreuzer et al. 1989; Teufel 1988; Abdullah et al. 1995).

U–Pb zircon data

Most of the zircon samples are discordant as shown by the projection of their U–Pb zircon data in Figs. 5–13. Some of the data points overlap within error or cluster around the concordia curve. The discordant data points plot on discordia lines intersecting the concordia curve between 476 and 496 Ma, with the lower intersections scattering between 0 and 45 Ma. There is thus no indication of a postmagmatic metamorphic overprint in the U–Pb zircon system. The Cambro-Ordovician age is interpreted to approximate the intrusion age of the mafic protoliths. The fan-shape cluster for the lower intersection has no geological meaning and probably indicates recent lead loss. A minor influence of the Variscan metamorphism and/or the pre-Variscan high-pressure event cannot be excluded. Similar discordant composition of zircons from mafic/ultramafic rock units have been reported by several authors (e.g. Oliver et al. 1993; von Quadt 1992; Hölzl and Köhler 1994; Bowes and Aftialon 1991) for other areas of the BM.

Several samples yielded data points which overlap the concordia curve. Some of these "concordant" samples (Figs. 5, 7, 8, 12), however, have distinct $^{206}Pb/^{238}U$ ages. In view of the relatively large errors, the presence of inherited lead in these samples cannot be excluded. The fact that the data points with the smallest analytical error do not plot on the curve probably points to the presence of inherited components.

Several single zircons (Table 5, nos. 2, 3, 29, 42) yielded concordant ages and apparently do not contain any old lead component. Abrasion of zircons enhanced the likelihood of obtaining concordant data points, if the abraded zircons contain no cores; however, the expectation for additional age information has not been confirmed.

In contrast to the multigrain analyses, the abraded grains as well as single zircon analyses show low and similar U concentrations. The U content of the zircons

Table 3 U–Th–Pb whole-rock data

Sample	U (ppm)	Pb (ppm)	Th (ppm)	$^{206}Pb/^{204}Pb$	Error	$^{207}Pb/^{204}Pb$	Error	$^{208}Pb/^{204}Pb$	Error	$^{207}Pb/^{204}Pb$ model age	μ-values	$^{206}Pb/^{204}Pb$	$^{207}Pb/^{204}Pb$	$^{208}Pb/^{204}Pb$	$^{238}Pb/^{204}Pb$	Th/U
												T-500	T-500	T-500		
VB 264	0.283	2.772	1.590	18.606	0.001	15.571	0.001	38.288	0.002	− 55	9.51	18.01	15.54	37.23	7.45	5.61
VB 280	0.290	2.881	1.580	18.565	0.001	15.573	0.001	38.329	0.002	− 17	9.53	17.97	15.54	37.32	7.34	5.44
VB 882	0.342	2.389	2.230	18.700	0.001	15.583	0.001	38.634	0.002	− 100	9.55	17.85	15.54	36.91	10.44	6.52
VB 911	0.449	4.012	2.040	18.735	0.002	15.581	0.001	38.389	0.003	− 133	9.53	18.07	15.54	37.45	8.16	4.54
VB 939	0.557	4.721	2.430	18.788	0.002	15.585	0.001	38.436	0.003	− 165	9.54	18.09	15.55	37.48	8.60	4.36
H 009	0.827	2.800	1.360	18.878	0.002	15.600	0.001	38.459	0.003	− 201	9.59	17.13	15.50	37.56	21.54	1.64
H 025a	0.245	2.900	0.460	18.315	0.002	15.561	0.001	37.918	0.003	151	9.53	17.82	15.53	37.63	6.16	1.87
H 025b	0.283	3.500	0.540	18.311	0.002	15.577	0.001	37.905	0.003	188	9.60	17.84	15.55	37.62	5.89	1.90
H 026	0.215	4.000	1.110	18.457	0.002	15.576	0.001	38.109	0.002	73	9.56	18.14	15.56	37.60	3.92	5.16
H 027	0.260	2.479	1.270	18.491	0.002	15.586	0.001	38.182	0.002	69	9.60	17.87	15.55	37.24	7.65	4.88
H 030	0.606	1.256	1.270	21.342	0.002	15.985	0.001	39.139	0.003	− 1146	10.86	18.35	15.81	38.50	35.19	2.09
H 031	1.030	17.26	0.412	18.736	0.002	15.606	0.002	38.502	0.004	− 76	9.64	18.32	15.58	38.22	4.35	0.40
H 033	1.239	1.68	0.578	19.687	0.002	15.628	0.001	39.733	0.003	− 779	9.60	17.22	15.49	38.49	53.79	0.46
H 034	0.681	6.357	1.433	20.750	0.001	15.742	0.001	39.162	0.002	− 1343	9.96	17.49	15.56	38.73	7.81	2.10
A 39	1.215	9.628	2.775	18.565	0.001	15.601	0.001	39.000	0.001	45	9.64	17.82	15.56	38.47	9.20	2.28
A 47	0.895	7.997	0.602	18.758	0.001	15.613	0.001	38.874	0.003	− 77	9.66	18.09	15.57	38.73	8.16	0.67

Table 4 Rb/Sr–Sm/Nd whole-rock/mineral data

Sample	Depths (m)	Rb (ppm)	Sr (ppm)	$^{87}Rb/^{86}Sr$	$^{87}Sr/^{86}Sr$	ε-Sr T-500	Sm (ppm)	Nd (ppm)	$^{147}Sm/^{144}Nd$	$^{143}Nd/^{144}Nd$	Error	T-DM	T-CH	ε-Nd T-0	ε-Nd T-500
39A5a	256	21	184	0.320	0.717032	150	8.45	40.87	0.1248	0.511538	6	2.78	2.34	− 21.5	− 16.9
47A4	326	49	213	0.647	0.711533	39.3	5.95	27.24	0.1318	0.512548	5	1.14	0.21	1.14	0.21
264	1260	13.8	313.1	0.124	0.704667	− 5.4	3.67	12.54	0.1768	0.512854	18	1.28	0.0	4.21	5.46
280	1340	15.6	215.9	0.210	0.702970	− 38.1	3.97	11.95	0.2005	0.512821	20	3.8	0.0	3.58	3.33
882	3610	13.0	279	0.131	0.703970	− 15.9	4.26	17.01	0.1512	0.512767	16	0.97	0.0	2.52	5.39
911	3718	18.0	151	0.099	0.704750	− 1.6	4.03	14.83	0.1642	0.512784	12	1.15	0.0	2.85	4.91
939	3835	17.0	181	0.264	0.704640	− 19.9	4.70	17.75	0.1597	0.512783	4	1.06	0.0	2.83	5.17
H009	4688	25.3	229.6	0.324	0.86912	2309	5.55	24.78	0.1352	0.512753	6	0.79	0.0	2.24	6.1
H025	6247	10.6	339.6	0.092	0.704254	− 8.01	1.24	4.56	0.1644	0.512773	6	1.19	0.0	2.63	4.70
H025	6245	19.9	282.1	0.205	0.704940	− 9.6	1.12	3.09	0.2184	0.512741	15	0.0	0.726	2.011	0.65
H026	6305	35.2	308.1	0.330	0.703737	− 39.4	2.63	9.20	0.1726	0.513003	8	0.58	0.0	7.12	8.64
H030	6670	7.66	73.4	0.293	0.721571	217	3.76	15.34	0.1479	0.512126	6	2.39	1.01	− 9.99	− 6.82
H031	7012	42	267	0.442	0.709256	27.6	1.43	6.58	0.1311	0.512388	8	1.43	0.58	− 4.87	− 0.69
H033	7405	8.0	303	0.074	0.736020	444	2.29	8.58	0.1609	0.511983	4	3.39	2.80	− 12.7	− 10.51
H034	8080	52	189	0.773	0.712411	38.9	1.97	9.42	0.1260	0.512427	6	1.27	0.46	− 4.12	0.40
280 garnet	Light						1.03	2.07	0.2996	0.513112	14				
280 garnet	Dark						1.09	2.23	0.2963	0.513103	15				
939 garnet							2.03	3.53	0.3474	0.513265	14				
911 garnet							1.939	4.505	0.2599	0.512869	16				

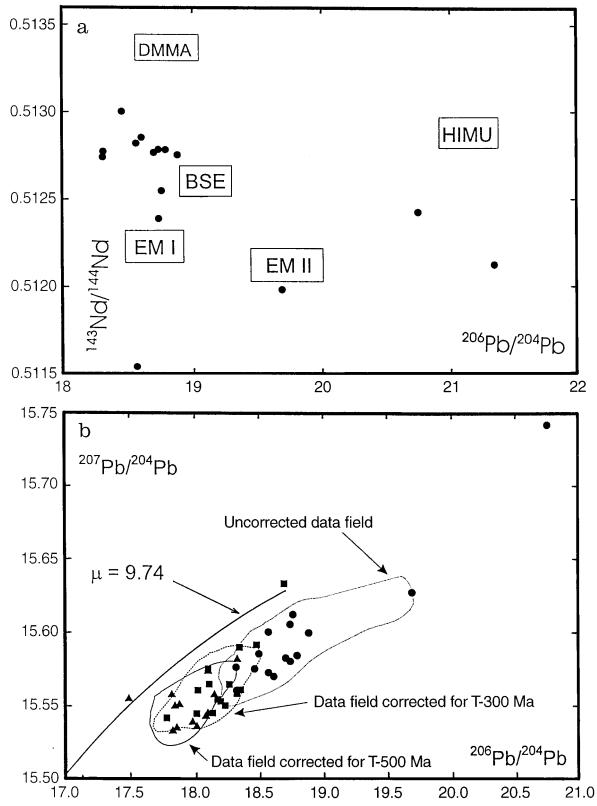

Fig. 4a Nd–Pb plot for the meta-gabbros, gneisses and amphibolites; **b** $^{206}Pb/^{204}Pb$ vs $^{207}Pb/^{204}Pb$ for mafic rocks and gneisses. The measured Pb ratios are corrected for T-300 and T-500 Ma

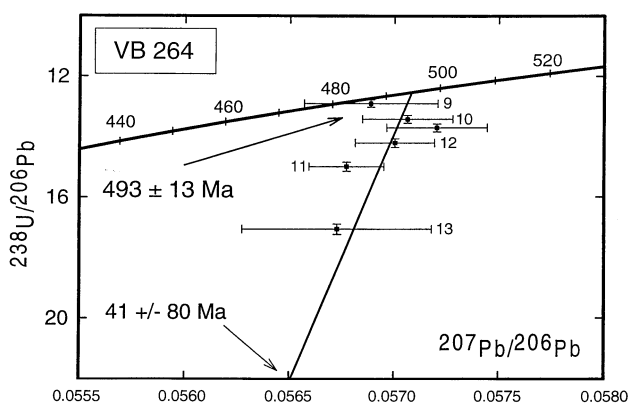

Fig. 5 $^{207}Pb/^{206}Pb$ vs $^{238}Pb/^{206}Pb$ plot for zircons from the meta-gabbro VB264, the numbers beside the data points refer to zircon fractions in Table 5

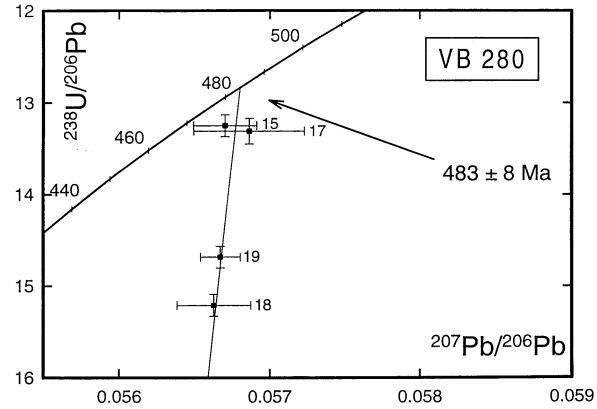

Fig. 6 $^{207}Pb/^{206}Pb$ vs $^{238}Pb/^{206}Pb$ plot for zircons from the meta-gabbro VB280

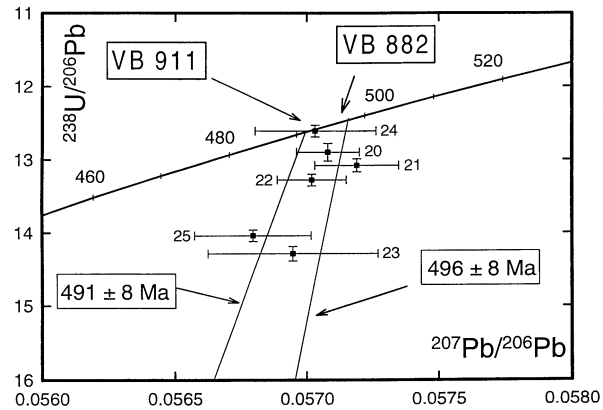

Fig. 7 $^{207}Pb/^{206}Pb$ vs $^{238}Pb/^{206}Pb$ plot for zircons from the meta-gabbro VB882/911

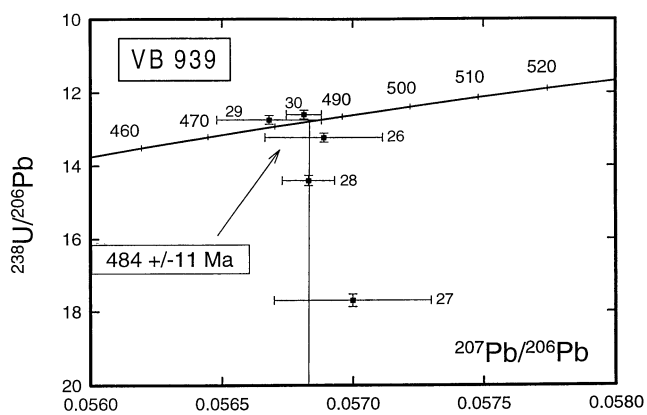

Fig. 8 $^{207}Pb/^{206}Pb$ vs $^{238}Pb/^{206}Pb$ plot for zircons from the meta-gabbro VB939

from the chlorite gneisses, which have high Zr, Nb and REE concentration (Table 2), is within the range of 185–240 ppm (Table 5).

The U of 200–900 ppm content of zircons from meta-gabbros is typical for mafic rocks (Oliver et al. 1993; von Quadt and Gebauer 1993), and the correlation between increase in U content and degree of discordancy is shown in Figs. 5–8 and Table 4.

The meta-gabbros of the VB (Figs. 5–8) and HB (Figs. 9–12) yield intrusion ages between 483 and

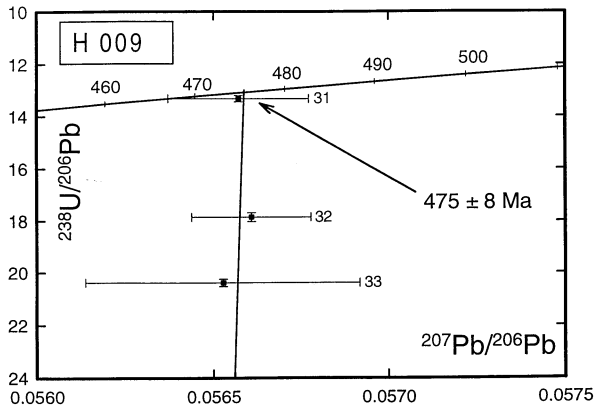

Fig. 9 $^{207}Pb/^{206}Pb$ vs $^{238}Pb/^{206}Pb$ plot for zircons from the meta-gabbro H009

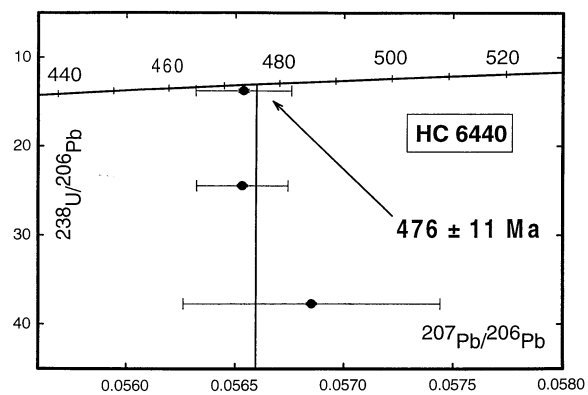

Fig. 10 $^{207}Pb/^{206}Pb$ vs $^{238}Pb/^{206}Pb$ plot for zircons from the meta-gabbro HC6440

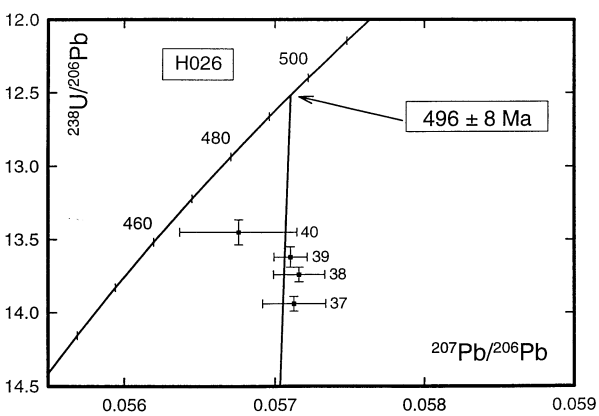

Fig. 11 $^{207}Pb/^{206}Pb$ vs $^{238}Pb/^{206}Pb$ plot for zircons from the meta-gabbro H026

496 Ma, whereas sample H009 yields an age of 475 Ma, which is 10 Ma younger. Within the analytical errors all meta-gabbros define a mean value of 490 $\pm$5.5 Ma. A major significant feature of the zircon data is the

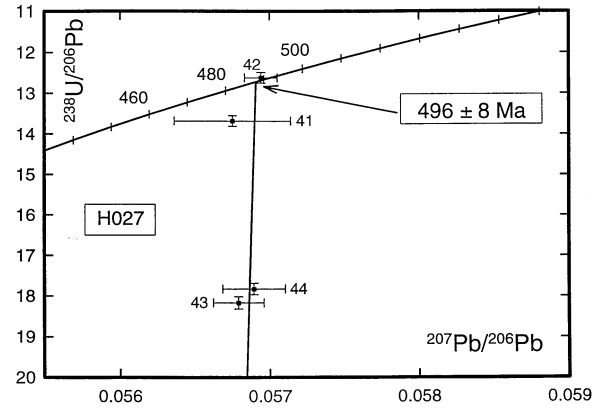

Fig. 12 $^{207}Pb/^{206}Pb$ vs $^{238}Pb/^{206}Pb$ plot for zircons from the meta-gabbro H027

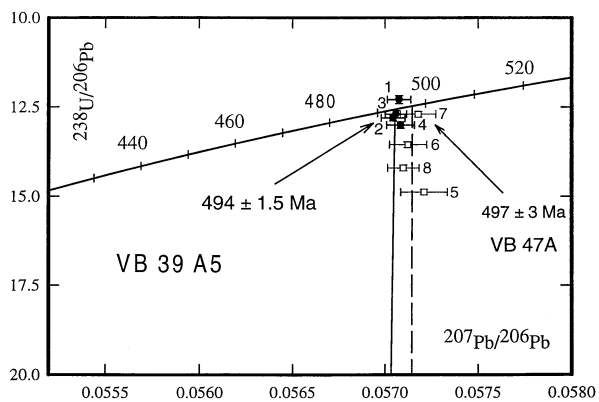

Fig. 13 $^{207}Pb/^{206}Pb$ vs $^{238}Pb/^{206}Pb$ plot for zircons from the gneisses 39A and 47B

spread of ages. This spread is either interpreted as a result of long magmatic activity or metamorphic processes which follow rapidly soon after crystallisation. O'Brien et al. (in press) reported a high pressure event, based on U–Pb zircon studies, in Ordovician time.

Discussion

Implication for the formation of mafic complex of the Bohemian massif

As shown in many studies, the U–Pb zircon method is well suited to obtain crystallisation ages of (poly-)metamorphosed igneous rocks. All analysed samples yielded at least one zircon fraction that was concordant within analytical errors, which demonstrates that any effects of postmagmatic disturbances can be minimised by selecting the most homogeneous core-free zircons for abrasion. Zircon can survive amphibolite-facies metamorphism, as long as no partial melting occurs in the rock.

Table 5 U–Pb analytical zircon data

	Sample	Fraction	U	Pb_{rad}	Pb_{com}	$^{206}Pb/^{204}Pb$	$^{206}Pb/^{238}U$	Error	$^{207}Pb/^{235}U$	$^{207}Pb/^{206}Pb$	Error	$^{238}U/^{206}Pb$	$^{206}Pb/^{238}U$	$^{207}Pb/^{235}U$	$^{207}Pb/^{206}Pb$	Corr
		(μm)	(ppm)	(ppm)	(ppm)											
1	39A5	Abraded	190	16.09	0.35	1606	0.08132	0.00019	0.6400	0.05708	0.00003	12.29	504	503	495	0.98
2	39A5	Abraded	221	18.72	0.29	1850	0.07812	0.00018	0.6145	0.05705	0.00009	12.05	485	485	493	0.97
3	39A5	Abraded	185	15.67	0.41	1220	0.07874	0.00017	0.6195	0.05706	0.00006	12.70	488	488	494	0.96
4	39A5	Abraded	198	16.76	0.44	1050	0.07692	0.00019	0.6055	0.05709	0.00009	13.05	478	478	495	0.98
5	47a	Abraded	213	15.11	0.95	784.8	0.06717	0.00012	0.5298	0.05721	0.00013	14.88	419	431	499	0.45
6	47a	Abraded	238	16.88	0.87	950	0.07380	0.00011	0.5813	0.05713	0.00010	13.55	459	465	496	0.85
7	47a	Abraded	192	13.62	0.65	1020	0.07840	0.00014	0.6208	0.05718	0.00009	12.70	487	490	499	0.95
8	47a	Abraded	185	13.12	0.45	1250	0.07042	0.00013	0.5544	0.05710	0.00009	14.20	439	448	495	0.97
9	264	> 110	331	30.28	5.54	304.1	0.07740	0.00071	0.6072	0.05689	0.00032	12.91	480	481	487	0.80
10	264	53–75	355	31.91	0.19	7126	0.07448	0.00144	0.5860	0.05706	0.00022	13.43	463	468	494	0.98
11	264	75–90	507	40.61	0.56	3435	0.06671	0.00026	0.5222	0.05677	0.00009	14.99	416	426	483	0.93
12	264	< 53	471	40.78	0.21	7476	0.07037	0.00015	0.5531	0.05700	0.00012	14.21	438	447	491	0.78
13	264	75–90	563	40.69	0.43	4596	0.05859	0.00589	0.4583	0.05673	0.00045	17.06	367	383	480	0.99
14	264	90–110	412	35.89	0.65	8627	0.07294	0.00032	0.5753	0.05721	0.00002	13.71	453	461	499	0.97
15	280	125–150	531	46.99	2.34	1067	0.07546	0.00078	0.5899	0.05670	0.00021	13.25	468	470	479	0.98
16	280	> 180	403	35.34	1.06	1764	0.07554	0.00166	0.5992	0.05753	0.00022	13.23	469	476	511	0.98
17	280	100–125	395	34.89	1.03	1758	0.07509	0.00170	0.5888	0.05686	0.00037	13.31	466	470	486	0.97
18	280	75–100	558	43.06	1.53	1500	0.06571	0.00094	0.5131	0.05663	0.00024	15.21	410	421	477	0.98
19	280	< 75	478	37.20	1.21	1674	0.06808	0.00071	0.5319	0.05667	0.00013	14.68	424	433	478	0.94
20	882	140–180	296	25.92	0.78	2580	0.07752	0.00089	0.6101	0.05708	0.00012	12.90	481	484	495	0.98
21	882	> 245	310	26.42	0.53	2707	0.07525	0.00152	0.5916	0.05702	0.00013	13.28	467	471	492	0.99
22	882	125–140	266	23.91	0.85	1382	0.07645	0.00079	0.609	0.05719	0.00016	13.08	474	479	498	0.99
23	911	> 125	534	40.58	1.76	1328	0.06995	0.00143	0.5493	0.05695	0.00032	14.29	435	445	490	0.98
24	911	> 125	502	42.79	2.66	945.9	0.07925	0.00167	0.6232	0.05703	0.00047	12.61	491	491	492	0.97
25	911	80–100	709	59.21	4.89	682	0.07121	0.00068	0.5576	0.05679	0.00022	14.04	443	450	484	0.96
26	939	< 45	697	67.54	5.4	524.1	0.07558	0.00029	0.5929	0.05689	0.00023	13.23	469	472	487	0.72
27	939	80–90	798	66.85	10.45	329.3	0.06801	0.00037	0.5345	0.05700	0.00030	17.70	424	434	491	0.74
28	939	> 125	712	54.77	1.65	4281	0.06940	0.00044	0.5438	0.05683	0.00003	14.40	432	440	485	0.99
29	939	80–90	652	60.28	2.25	1010	0.07837	0.00082	0.6125	0.05668	0.00020	12.75	486	485	479	0.98
30	939	< 53	631	61.23	7.30	422	0.08289	0.00013	0.6494	0.05681	0.00007	12.06	513	508	484	0.97
31	H009	72–90	361	29.73	1.044	1549	0.07512	0.00043	0.5859	0.05657	0.0002	13.31	466	468	475	0.98
32	H009	95–100	321	19.59	0.556	1865	0.05601	0.00058	0.4372	0.05661	0.0002	17.85	351	368	477	0.98
33	H009	> 100	303	16.11	0.199	3833	0.04905	0.00035	0.3823	0.05653	0.0004	20.38	308	328	473	0.99
34	HC	6439	257	11.13	0.606	1072	0.04086	0.00054	0.3185	0.05653	0.0002	24.47	258	280	474	0.97
35	HC	6441	284	20.94	1.25	1034	0.07256	0.00076	0.5657	0.05654	0.0002	13.78	451	455	474	0.97
36	HC	6443	307	8.294	0.497	973	0.02648	0.00013	0.2076	0.05685	0.0006	37.76	168	192	486	0.97
37	H026	< 53	756	61.48	18.61	200	0.07169	0.00086	0.5647	0.05713	0.00011	13.94	446	455	496	0.82
38	H026	120–150	595	48.77	8.02	315	0.07278	0.00013	0.5736	0.05716	0.00081	13.74	453	460	497	0.88
39	H026	70–90	511	42.19	6.91	352	0.07344	0.00018	0.5783	0.05710	0.00022	13.62	457	463	495	0.90
40	H026	> 230	922	74.57	20.96	222	0.07429	0.00049	0.5813	0.05676	0.00053	13.46	462	465	482	0.84
41	H027	180–250	299	22.66	2.519	554	0.07308	0.00077	0.5718	0.05675	0.00039	13.68	455	460	482	0.95
42	H027	Abraded	195	16.14	0.014	19601	0.07925	0.00007	0.6222	0.05694	0.00011	12.62	491	491	490	0.99
43	H027	100–175	265	15.02	0.741	1229	0.05502	0.00056	0.4308	0.05679	0.00017	18.17	345	363	483	0.97
44	H027	75–90	230	13.18	0.730	1074	0.05609	0.00029	0.4353	0.05689	0.00021	17.83	351	367	464	0.97
45	HC9100	Cutting	1314	106.98	5.19	636	0.08489	0.00013	0.6920	0.05911	0.00019	11.78	525	534	571	0.95

A paleo-tectonic reconstruction of the pre-Variscan evolution of the Bohemian massif (BM) leads to a subduction and an enrichment process of the mantle material. The degree of contamination of the mantle with Cadomian crust can only be speculated on, but some contamination is indicated by the Nd–Sr–Pb isotope pattern and the $^{207}Pb/^{204}Pb$ vs $^{206}Pb/^{204}Pb$ diagram. The magmatic ages determined for the meta-gabbros from the KTB introduce an additional puzzle in understanding the pre-Variscan evolution of the BM. The existence of a pre-Variscan basement in the BM was detected by zircon U–Pb analyses. The oldest component is found in zircons from paragneisses of the Regensburger Wald. Gebauer et al. (1989) used the SHRIMP to detect a 3.8 Ga old zircon component. Further ages at 2.4–2.6 and 1.9–2.2 Ga point to geological events which probably belong to the evolution of the Gondwana continent as those data are unknown from the northern continent Laurentia.

With the breakup of the Gondwana supercontinent at the end of the Proterozoic a long period of volcanism started and erosion products of the uplifted Cadomian basement filled sedimentary basins. The timing of this magmatic event within the BM was established by Gebauer and Grünenfelder (1979) at $525 \; +40/-31$ Ma (Münchberg gneiss complex), at 525 ± 11 Ma (ZEV; Teufel 1988), at 511 ± 3 Ma (Hohe Bogen; Gebauer 1993) and at 494 ± 1 Ma (Marianske Lasne; Bowes and Aftialon 1991). The latter age is supported by the ages of the KTB bore hole profile (Figs. 5–13). The very scarce outcrops of mafic rocks within the BM are composed of meta-gabbros, amphibolites, serpentinites and pyroxenites. The felsic magmatism that also belongs to the rifting event is possibly documented by orthogneisses; Teufel (1988) dated an amphibolitic orthogneiss of the ZEV at 530 Ma and a granitic orthogneiss from Böhmisch Bruck shows similar intrusion ages (D. Gebauer, pers. commun.).

Several granitoid rocks from other tectonic units yielded intrusion ages which fit within the time of breakup of Gondwana. The granitoids from the Erzgebirge intruded between 550 and 555 Ma (Kröner et al. 1994) and the Lusatian granitoids show a range of zircon Pb–Pb ages between 542 and 587 Ma (Kröner et al. 1994). In the region of SW Poland the granitoids are younger and were dated at 482–487 Ma (Kröner et al. 1994) and at 488–504 Ma (Oliver et al. 1993). Most of these granitoid rocks are older than the mafic magmatism in Cambro-Ordovician time and therefore represent one possible member (ε-Nd_{T550}: -3.7 to -7.7) for contamination of the mafic source with a continental crustal source.

Constraints on source rocks – mantle-crust mixing

Only few geochemical/isotope-geochemical data of mafic rocks of the BM are available. The ε-$Nd_{T\text{-}500}$ values of the meta-gabbros of the KTB (Table 4), of eclogites from Winklarn (von Quadt and Gebauer 1993), of eclogites from Münchberger gneiss massif (Stosch and Lugmair 1990), of mafic rocks from Neukirchen (Miethig 1995) and mafic rocks from the Saxonian granulite massif (von Quadt 1993) show a wide range from $+8.5$ to $+1.2$. This observation is not surprising in young and multiply overprinted and mixed source material.

The geochemical and isotope-geochemical data of the mafic rocks point to an enriched source, which is characterised by high contents of LREE, Pb, Sr, K, U, Th, Ba and Rb. Based on the pattern of enrichment (Fig. 2; Table 3) one possible cause is contamination of the mantle by subducted sediments or by assimilation of Cadomian crust. However, the Th/U ratios (Table 3) exclude a possible component from the lower continental crust. Only a few mafic rocks reflect the existence of a depleted mantle component. Based on their characteristic Sr–Nd–Pb isotope patterns, Uyeda (1982) favoured a tectonic regime above subduction zones which leads to a tensional stress across the arc-trench gap. This causes subsidence of the trench so that the sediments are efficiently subducted. Probably only a few remnants of this mafic crust are tectonically emplaced into the continental crust and intercalated with continental crust. The fact that only very few relics of the mafic crust of the pre-Variscan evolution have been discovered leads to one speculation that most of these were subducted.

The denudation of such mafic relics is related in variable degree of erosion and/or tectonic processes. Determining the time when the Cambro-Ordovician sedimentary troughs were closed is difficult. Minimum ages are indicated by ages of metamorphism and these are up to Silurian (423 Ma; von Quadt and Gebauer 1993; Gebauer 1991), Devonian (380–395 Ma; Stosch and Lugmair 1991; Gebauer and Grünenfelder 1979; von Quadt 1994) and Carboniferous metamorphic ages. On the basis of data, it is difficult to establish if there are several subcycles of metamorphism which could reflect a gradual closing of the sedimentary basin. In contrast to other parts of the European Variscides, no Ordovician high-pressure metamorphism has been detectable. If the interpretation of P. O'Brien (pers. commun.) is correct, a first hint of an Ordovician high-pressure event combined with a subduction process was detected. The observation that Cambro-Ordovician metamorphic ages exist within the same rock formation suggests the existence of Cambro-Ordovician subduction. If subduction and uplift rates of >10 km/Ma (10 mm/year) are assumed (Baldwin et al. 1990), the complete orogenic cycle could have taken place within a time span of 10 Ma. The zircon U–Pb results do not contradict such a process. Together with the Cambro-Ordovician protolith ages the geochronological investigation of paragneisses of the BM point to an Ordovician metamorphic event.

A simple two-step mixing model calculation between a depleted mantle member (ε-$Nd_{T500} = 8.5$, Nd = 9.2 ppm, $^{207}Pb/^{204}Pb = 15.4$, Pb = 0.5 ppm) and continental crust (ε-$Nd_{T500} = -10$, Nd = 20 ppm, $^{207}Pb/^{204}Pb = 15.70$, Pb = 12 ppm), as determined for the Lusatian block (Kröner et al. 1994) show for the Nd isotopes as well as for the Pb isotopes that an admixture of 5–10% continental crust is required to reduce the ε-Nd value from +8.5 to +5 and an increase in the $^{207}Pb/^{204}Pb$ ratio from 15.4 to 15.56.

Comparison of U–Pb zircon data of the variegated group and basic group

The magmatic intrusion ages of mafic rocks from different b-units (Hirschmann et al. 1994) within the KTB profile do not pertain to the magmatic evolution of the gneiss units (g unit) and variegated units (v unit). Further information for the g units are given by Grauert et al. (1994) and Söllner et al. (1994 and this volume). The v unit of the KTB profile consists of amphibolites, gneisses, calcsilicate gneisses and biotite gneisses (Hirschmann et al. 1992). Two chlorite gneisses extremely enriched in Nb and Zr (Table 2) were selected for U–Pb zircon analyses. Based on morphology and cathodoluminescence studies these zircons seem to represent a magmatic type. The calculated U–Pb ages of 494 and 497 Ma (Fig. 13; Table 5) are comparable with those from Söllner et al. (1994 and this volume) and are interpreted, in contrast to Söllner et al. (1994), to reflect the time of a felsic magmatism within the v units. Based on investigations by P. O'Brien (pers. commun.) the Cambro-Ordovician event comprises a magmatic and a metamorphic event related to a subduction scenario. The existence of mafic and felsic magmatism does not argue against a subduction scenario. If the magmatism of the b and v units took place at different localities, the tectonic intercalation for the observed profile of the KTB was probably the result of the Devonian compression event. There are no indications for such processes in post-Devonian time.

Conclusion

Nd–Pb isotope composition of the meta-gabbros clearly demonstrates that the assumption of a uniform source region is unrealistic. Instead, the ε-Nd_T values were acquired by interaction of mantle and crustal components. The Nd–Pb studies allow distinguishing of (a) a mantle end member and (b) continental Cadomian crust, as the other end member. No Archean crustal material is detectable.

U–Pb zircon investigation of meta-gabbros from different levels of the KTB profile are best interpreted by a magmatic event in Cambro-Ordovician time. U–Pb zircon analyses of two chlorite gneisses from the v unit suggests the existence of a simultaneous felsic magmatism in Cambro-Ordovician time.

The existence of a magmatic event within the b and v unit leads to an interpretation that both events took place within the same tectonic setting; the tectonic stacking of the two units occurred in Devonian time during the subduction process.

Acknowledgements The author thanks J. Ridley and V. Köppel for their critical and constructive comments, and two anonymous reviewers for their useful comments on this manuscript. He also thanks W. Wittwer and R. Aubert for assistance in mineral separation.

References

Abdullah N, Grauert B, Krohe A, Lork A, O'Brien P (1995) Ages of polymetamorphism in rocks from the German deep drilling hole (KTB), eastern Bavarai. Terra Nova (Suppl) 7:352

Aftialion M, Bowes DR, Vrana S (1989) Early Carboniferous U–Pb ages for garnetiferous perpotassic granulites, Blansky les massif, Czechoslovakia. N Jahrb Mineral Mh 4:145–152

Ahrendt H, Glodny J, Henjes-Kunst F, Höhndorf A, Kreuzer H, Küstner W, Müller-Sigismund H, Schüssler U, Seidel E, Wemmer K (1997) Rb–Sr and K–Ar mineral data of the KTB and the surrounding area and their bearing on the tectonothermal evolution of the metamorphic basement rocks. Geol Rundsch 86, Suppl: S251–S257

Baldwin SL, Hill EJ, Lister GS, McDougall IM, Ireland T (1990) P–T–t history of a young orogenic belt, D'Entrecasteaux island, Papua New Guinea. Annu Rep Aust Nat Uni, pp 36–37

Beard BL, Medaris LG, Johnson CM, Misar Z, Jelinec E (1991) Nd and Sr isotope geochemistry of Moldanubian eclogites and garnet peridotites, Bohemian massif (CSFR). Abstr 2nd Int Eclogite Field Symp Oxford 1991. Terra Nova 3 (Suppl 6):4

Blümel P (1983) The western margin of the Bohemian massif in Bavaria. Fortschr Mineral Beih 62 (2):171–199

Blümel P (1984) Mitteldruck- und Niederdruckmetamorphose in den ausseralpinen Varisziden Mitteleuropas. Fortschr Mineral Abh Beih 62 (1):28–29

Bowes DR, Aftialon M (1991) U–Pb zircon isotopic evidence for early Ordovician and late Proterozoic units in the Marianske Lazne complex, Central European Hercynides. N Jahrb Miner Mh H7:315–326

Gebauer D (1991) Two Paleozoic high-pressure events in a garnet–peridotite of northern Bohemia, Czechoslovakia. Terra Nova 3 (Suppl 6):5

Gebauer D (1993) Geochronologische Übersicht. In: Geologische Karte von Bayern 1:25 000. Erl Zu Blatt Nr 6439 Tännesberg, Bayerisches Geol Landesamt, Müchen

Gebauer D, Grünenfelder M (1978) U–Pb zircon and Rb–Sr mineral dating of eclogites and their country rocks. Example: Münchberg Gneiss massif, NE Bavaria. Earth Planet Sci Lett 42:35–44

Gebauer D, Williams IS, Compston W, Grünenfelder M (1989) The development of the Central European continental crust since the Early Archean based on conventional and ion-microprobe dating of up to 3.84 Ga old zircons. Tectonophysics 157:81–96

Goldstein SL, O'Nions RK, Hamilton PJ (1984) An Sm–Nd isotopic study of atmospheric dusts and particulates from major river systems. Earth Planet Sci Lett 70:221–236

Grauert B, Hänny R, Soptrajanova G (1974) Geochronology of a polymetamorphic and anatectic gneiss region: the Moldanubicum of the area Lam-Deggendorf, eastern Bavarian Germany. Contrib Mineral Petrol 45:37–63

Hirschmann G, Lich S, Wall H de (1994) KTB Oberpfalz – einige Ergenisse der geowissenschaftlichen Bearbeitung. Zbl Geol Paläont Teil I H7 (8):861–873

Hirschmann G, Stennet G, Rohrmüller J (1994) The lithological units of the ZEV. KTB Report 94–3 : 63–74
Henjes-Kunst F, Höhndorf A, Kreuzer H, Seidel E (1994) K/Ar and Ar/Ar dating on minerals of the KTB. KTB Rep 94–2 : B33
Hölzl S, Köhler H (1994) Zirkondatierungen an Gesteinen der KTB. KTB Rep: 94–2 : B35
Kreuzer H, Okrusch M, Raschka H, Schüssler U, Seidel E, Vejnar Z (1989) Ar/Ar Datierungen am NW-Rand der Böhmischen Masse. KTB Rep 89–3 : 426
Kröner A, Jaeckel P, Opletal M (1994) Pb–Pb and U–Pb zircon ages for orthogneisses from eastern Bohemia: further evidence for a major Cambro-Ordovician magmatic event. J Czech Geol Soc 39 (1) : 61
Kröner A, Hegner E, Jaeckel P (1994) Pb–Pb and U–Pb zircon ages and Nd isotopic systematics for metamorphic rocks from the Gory Sowie block, West Sudetes, Poland, and geodynamic significance. J Czech Geol Soc 29 (1) : 60
Kröner A, Hegner E, Hammer J, Haase G, Bielicki KH, Krauss M, Eidam J (1994) Geochronology and Nd–Sr systematics of Lusatian granitoids: significance for the evolution of the Variscan orogen in east–central Europe. Geol Rundsch 83 : 357–376
Kröner A, Willner AP, Hegner E, Frischbutter A, Hofmann J, Bergner R (1995) Latest Precambriam zircon ages, Nd isotopic systematics and P–T evolution of granitoid orthogneisses of the Erzgebirge, Saxony and Czech republic. Geol Rundsch 84 : 437–456
Ludwig KR (1980) ISOPLOT, version 2.03, USGS Open File Rep 88–557, rev 1990
Manshes G, Allégre CJ, Provost A (1984) U–Th–Pb systematics of the eucrite "Juvinas": precise age determination and evidence for exotic lead. Geochim Cosmochim Acta 48 : 2247–2264
Miethig A (1995) Sr- und Nd-Isotopensystematik an den Gesteinen der Gabbroamphibolitmasse von Neukirchen bei Hl. Blut-kdyne. Dissertation, Univ München, 206 pp
O'Brien P, Duyster J, Grauert B, Schreyer W, Stöckert B, Weber K (1997) Crustal evolution of the KTB drill site: from oldest relics to the late Hercynian granites. J Geophys Res (in press)
Oliver GJK, Corfu F, Krogh TE (1993) U–Pb ages from SW Poland: evidence for a Caledonian suture zone between Baltica and Gondwana. J Geol Soc Lond 150 : 355–369
Pearce JA (1982) Trace element characteristics of lava from destructive plate boundaries. In: Thorpe RS (ed) Andesites: orogenic andesites and related rocks. Wiley, New York, pp 525–548
Pearce JA, Norry MJ (1979) Petrogenetic implications of Ti, Zr, Y and Nb variations in volcanic rocks. Contrib Mineral Petrol 69 : 33–47
Quadt A von (1990) U–Pb zircon and Sm–Nd analyses on metabasites from the KTB pilote bore hole. KTB Rep 90–4 : 545
Quadt A von (1992) U–Pb zircon and Sm–Nd geochronology of mafic and ultramafic rocks from the central part of the Tauern Window (eastern Alps). Contrib Mineral Petrol 110 : 57–67
Quadt A von (1993) The Saxonian Granulite massif: new aspects from geochronological studies. Geol Rundsch 82 : 516–530
Quadt A von (1994) Mafic/ultramafic units of the continental deep drilling site: a multi element approach. KTB Rep 94–2 : B15
Quadt A von, Gebauer D (1993) Sm/Nd and U/Pb dating of eclogites and granulites from the Oberpfalz, NE Bavaria. Chem Geol 109 : 317–339
Richard P, Shimizu N, Allegre CJ (1976) $^{143}Nd/^{146}Nd$, a natural tracer: an application to oceanic basalts. Earth Planet Sci Lett 31 : 269–278
Siebel W, Höhndorf A, Wendt I (1995) Origin of late Variscan granitoids from NE Bavaria, Germany, exemplified by REE and Nd isotope systematics. Chem Geol 125 : 249–270
Söllner F, Loske W, Miller H (1994) Subdivision of the KTB series (Germany) according to variations in provenance and thermal history of zircons in paragneisses: evidence from U–Pb zircon dating. N Jahrb Mineral Mh H8 : 337–357
Söllner F, Miller H (1994) U–Pb systematics on zircons from chlorite gneiss of metavolcanic layer V4 (7260–7800 m) from the KTB-Hauptbohrung. KTB Rep 94–2 : B31
Söllner F, Nelson D, Miller H (1997) Provenance and thermal history of gneiss series from the KTB drill hole (Germany): evidence from SHRIMP- and conventional U–Pb age determinations on zircons. Geol Rundsch 86, Suppl: S235–S250
Steiger RH, Jäger E (1977) Subcommision on geochronology: convention on the use of decay constants in geo- and cosmochronology. Earth Planet Sci Lett 36 : 359–362
Stosch HG, Lugmair GW (1990) Geochemistry and evolution of MORB-type eclogites from the Münchberg Massif/southern Germany. Earth Planet Sci Lett 99 : 230–249
Teufel S (1988) Vergleichende U–Pb- und Rb–Sr-Altersbestimmungen an Gesteinen des Uebergangsbereichs Saxothuringikum/Moldanubikum, NE-Bayern. Göttinger Arb Geol Paläont 35 : 87
Wemmer K, Ahrendt H (1994) Age determination on retrograde processs and investigations on blocking conditions of isotope systems of KTB rocks. KTB Rep 94–2 : B32
Zindler A, Hart S (1986) Chemical geodynamics. Ann Rev Earth Planet Sci 14 : 493–571